Preprint typeset in JHEP style - HYPER VERSION

Dyonic Black Hole and Holography

Suvankar Dutta*, Akash Jain† and Rahul Soni‡

Department of Physics
Indian Institute of Science Education and Research Bhopal
Bhopal 462 023
India

Abstract: We study thermodynamic properties of dyonic black hole and its dual field theory. We observe that the phase diagram of a dyonic black hole in constant electric potential and magnetic charge ensemble is similar to that of a Van der Waals fluid with chemical potential. Phase transitions and other critical phenomena have been studied in presence of magnetic charge and chemical potential. We also analyse magnetic properties of dual conformal field theory and observe a $ferromagnetic$ like behavior of boundary theory when the external magnetic field vanishes. Finally, we compute susceptibility of different phases of boundary CFT and find that, depending on the strength of the external magnetic field and temperature, these phases are either paramagnetic or diamagnetic.

*suvankar@iiserb.ac.in
†akash@iiserb.ac.in, ajainphysics@gmail.com
‡rahulsoni@iiserb.ac.in, rahulsoni.phy@gmail.com

Contents

1. Introduction and summary

Recently there has been much interest in holographic study of condensed matter systems. Different properties of (d+1) dimensional condensed matter systems (field theories) are being studied from the perspective of string theory. In this paper we attempt to understand magnetic properties of a $(2+1)$ dimensional system via the AdS/CFT correspondence (proposed by Maldacena in 1997 [1, 2]). For that, we consider a (3+1) dimensional *dyonic* black hole spacetime as our bulk system.

Thermodynamic properties of electrically charged black holes in arbitrary dimensions are well studied in the literature. However, in four spacetime dimensions, because of electromagnetic duality, it is possible to construct a black hole which carries both electric and magnetic charges. Such black hole solution is called dyonic black hole. In this work we consider a dyonic black hole in asymptotically AdS spacetime, as we aim to understand thermodynamic properties of its dual boundary CFT.

A dyonic black hole sources two different fields: graviton (metric) and a $U(1)$ gauge field. The metric satisfies asymptotic AdS boundary conditions and for gauge field there are two possible fall-off conditions. A normalizable mode that corresponds to a VEV of the dual operator (an R-current), and a non-normalizable mode corresponding to the application of an external gauge field, which deforms the boundary theory. The deformed (2+1) dimensional field theories have drawn enough attention recently in the context of a holographic understanding of condensed matter phenomena like superconductivity/superfluidity [3], the Hall effect [4], magnetohydrodynamics [5], the Nernst effect [6] and more.

On the other hand in the bulk theory, presence of a magnetic monopole enriches the phase diagram of black holes in AdS spacetime. In [7], the authors studied electrically charged AdS black holes in diverse dimensions. They found a seemingly surprising similarity between phase diagrams of black hole and Van der Waals fluid. Considering the black hole in a fixed electric charge ensemble it was observed that identifying β, q and r_+ (inverse temperature, electric charge and horizon radius of black hole respectively) with the pressure, temperature and volume of liquid-gas respectively, black hole phase diagram is similar to that of a non-ideal fluid described by the Van der Waals equation. Below a critical value of electric charge, there exists three different phases/branches of black hole. These three different branches have different horizon radii. The smallest one is identified with the liquid state and the largest one is identified with the gaseous state of Van der Waals fluid. Whereas, the medium size unstable black hole is identified with

the un-physical state of Van der Waals fluid. In stead of fixed charge ensemble, if we consider the black hole in fixed electric potential ensemble, the similarity between the phase diagrams goes away.

The same system has also been studied by [8][1]. In this interesting paper the authors identified the negative cosmological constant with thermodynamic pressure of the black hole and volume covered by the event horizon to be the thermodynamic volume conjugate to pressure (following [10]). Under this consideration, the phase diagram of black hole in canonical ensemble exactly matches with the phase diagram of the Van der Waals fluid (no need to make any ad-hoc identification between the parameters like [7]). But, in this picture the black hole phase diagram has an extra parameter: electric charge. Therefore, phase transitions and other critical phenomena depend on this extra parameter. However, in grand canonical ensemble the similarity between the phase diagrams is lost again. Higher derivative generalization of black hole phase diagram has been studied in [11].

We consider a dyonic black hole in $(3+1)$ dimensions and find that black hole phase diagram is more colorful. We observe that putting the black hole in constant electric and magnetic charge ensemble one gets the same result of [7, 8] only $q_E^2 \to q_E^2 + q_M^2$. However, if we consider the black hole in constant electric potential ensemble (keeping magnetic charge arbitrary) then unlike [7, 8], we get a phase diagram which is same as liquid-gas phase diagram with a chemical potential. Therefore, in this case phase transitions and different critical behaviour depend on temperature, volume, pressure, magnetic charge and the electric potential. In other words, the black hole phase diagram is more rich and our aim is to explore different parts of this phase diagram which have not been studied before. We summarize our results below in section 1.1.1.

In the context of the AdS/CFT correspondence, the dyonic black hole is dual description of a $(2+1)$ dimensional CFT with a conserved $U(1)$ charge ($\sim q_E$) and in a constant magnetic field ($\sim q_M$). Field theory in presence of external electromagnetic field displays many interesting behaviours. The second part of this paper is devoted to study magnetic properties of different phases of the boundary CFT. We find a *'ferromagnetic'* like behaviour of boundary theory. We observe that in the limit $B \to 0$ the magnetization of the system vanishes beyond a critical temperature, whereas below that temperature it attains a constant value. However, unlike ferromagnetism there is a sharp jump in the magnetization at the critical value.

[1] See also [9].

1.1 Summary of main results

Here we summarize the main results of this paper.

1.1.1 Black hole phase diagram

We study thermodynamic properties of dyonic black hole in constant electric potential and magnetic charge ensemble. Identifying $-\Lambda$ as the thermodynamic pressure and its dual as thermodynamic volume, we see that the system shows almost similar phase diagram as in [8], but its parameter space is more rich.

The phase diagram of dyonic black hole in constant electric potential has been depicted in figure (3a) and figure (3b). Here we see that for a fixed $\Phi_E < 1$ and $q_M < q_{M(c)}$ there exists a critical temperature T_c below which the black hole has three different phases inside a particular window along P axis. We call them *small black hole* (SBH), *medium black hole* and *large black hole* (LBH) (according to size V). This phase diagram shows a qualitative similarity with liquid-gas phase diagram governed by the Van der Waals equation. However, the black hole equation of state (see equation (4.1)) is different than the Van der Waals equation. We shall see in section 4 that unlike Van der Waals fluids, black hole phase diagram is controlled by two extra parameters Φ_E and q_M (apart from usual P, T and V). Hence, critical points and phase transitions in this phase diagram depend on the values of these two extra parameters as well.

We calculate the free energy of this system and observe that inside some region in parameter space ($q_M - \Phi_E$ plane), there exists a phase transition between large black hole to small black hole as we decrease temperature. High temperature phase is governed by large black hole whereas low temperature phase is dominated by small black hole. If we are outside that region then the only thermodynamically stable phase is the large black hole phase.

In $q_M \to 0$ limit, the large black hole to small black hole phase transition reduces to the Hawking-Page phase transition. In this case the small black hole evaporates and the low temperature phase is dominated by a global AdS.

1.1.2 Holography with dyonic black hole: Magnetic properties of boundary theory

We study the magnetic properties of a (2+1) dimensional boundary CFT. The free energy of the CFT is conjectured to be the free energy of the bulk spacetime. We calculate magnetization of the CFT and find that in $B \to 0$ limit the boundary theory shows a ferromagnetic like behaviour. Above a temperature T_o the dominant phase has zero magnetization whereas below T_o a constant magnetization phase is dominant (see figure (1)). Unlike a ferromagnetic system though, we find a discontinuity in magnetization at T_0. In presence of a finite magnetic field we calculate susceptibility χ of the system and

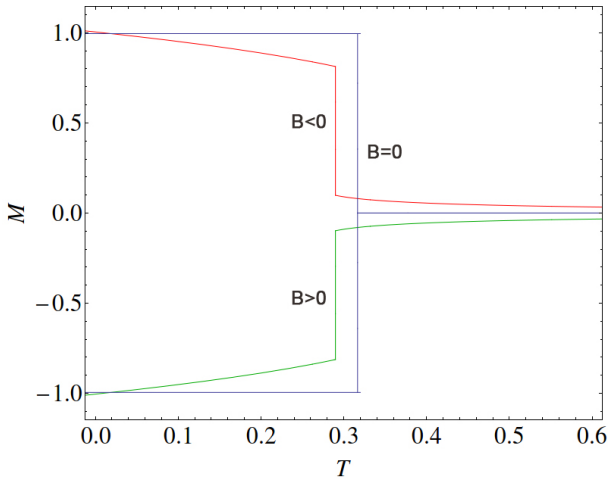

Figure 1: $\mathcal{M}$ vs. T curve for $B \to 0$ (blue curve) and $B \neq 0$ (red and green curve for $B < 0$ and $B > 0$ respectively). At the transition temperature a sharp jump in magnetization is observed. Low temperature phase has constant magnetization and high temperature phase has zero magnetization.

observe diamagnetic ($\chi < 0$) or paramagnetic ($\chi > 0$) behavior of the system depending on the temperature and magnetic field. We brief our observation here and present the details in section 5.

- There exists a maximum magnetic field B^* above which the thermodynamics is dominated by a diamagnetic phase for any temperature. This phase of CFT is dual to the single black hole phase in the bulk. See figure (2a).
- For $B_c < B < B^*$ (B_c is the critical magnetic field), the thermodynamics is again governed by a single phase (which is dual to the single black hole phase in bulk). But this phase shows two crossovers between diamagnetic and paramagnetic phases.

Very high and very low temperature phases are diamagnetic, while in between the system is paramagnetic. See figure (2b).

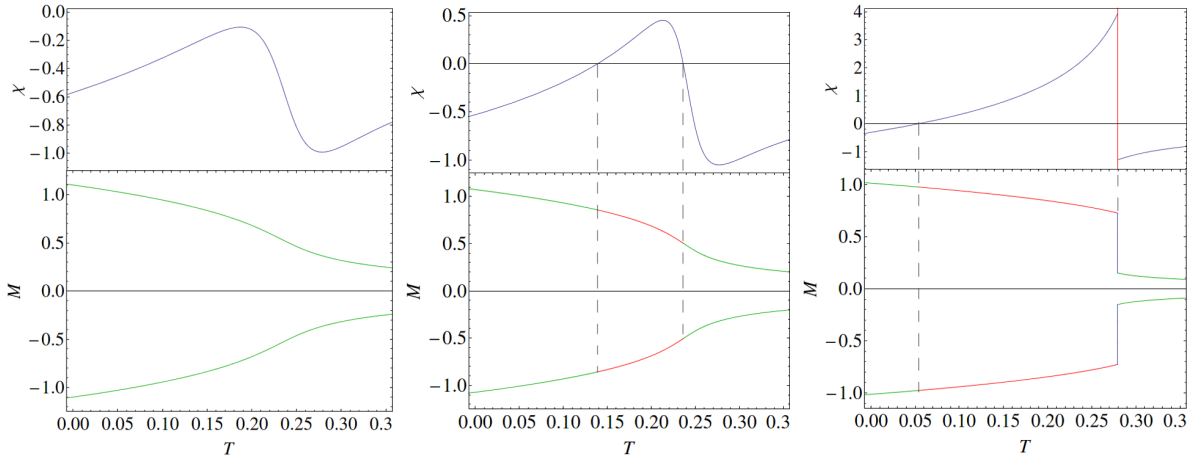

(a) $B > B^*$. **(b)** $B^* > B > B_c$. **(c)** B sufficiently less than B_c.

Figure 2: $\chi - T$ and $\mathcal{M} - T$ plots. Green segments are diamagnetic while red are paramagnetic. In plot **(c)** the transition from large magnetization phase to small magnetization phase is a transition from a paramagnetic phase to a diamagnetic phase.

- Criticality appears at $B = B_c$. Two new phases nucleate (one of which is thermodynamically unstable). Other two stable phases are dual to small and large black holes in bulk. If B is sufficiently smaller that B_c, we see a transition between a paramagnetic (dual to SBH) phase and diamagnetic (dual to LBH) phase at $T = T_0$. See figure (2c).

The organisation of this paper is as follows. In the next section we give a quick review of dyonic black hole and its holographic set-up. In section 3, we discuss different phases of dyonic black hole and their thermodynamic properties. Phase transitions and phase diagrammes have been studied in section 4. Section 5 contains discussion on magnetic properties of the dual CFT. Stability analysis has been studied in section 6. We conclude our paper with some remarks in section 7. There are four appendices in this paper. In appendix A, we provide an alternative method to calculate black hole free energy: background subtraction method. Appendix B contains a through discussion on critical points in $\mathcal{M} - B$ plane. We study symmetry properties of the free energy of the boundary theory in appendix C. In the last appendix (appendix D), we provide a detailed study on diamagnetic and paramagnetic phases of the CFT.

2. Dyonic black hole solution

AdS dyonic-dilaton black hole solution can be embedded into maximal gauged supergravity in four dimensions [12]. However, we consider a rather simpler solution, which solves the equations of motion obtained varying the Reissner-Nordström action in four dimensions in presence of a cosmological term.

We start with the Reissner-Nordström action in presence of a negative cosmological constant,

$$I = \frac{1}{16\pi G_4}\int \mathrm{d}^4x\sqrt{g}\left(-R + F^2 - \frac{6}{b^2}\right). \tag{2.1}$$

The Equations of Motion are given by,

$$R_{\mu\nu} - \frac{1}{2}g_{\mu\nu}R - \frac{3}{b^2}g_{\mu\nu} = 2(F_{\mu\lambda}F_{\nu}{}^{\lambda} - \frac{1}{4}g_{\mu\nu}F_{\alpha\beta}F^{\alpha\beta}); \tag{2.2}$$

$$\nabla_\mu F^{\mu\nu} = 0. \tag{2.3}$$

A static spherically symmetric solution to these equations is given by

$$A = \left(-\frac{q_E}{r} + \frac{q_E}{r_+}\right)\mathrm{d}t + (q_M\cos\theta)\,\mathrm{d}\phi \tag{2.4}$$

and

$$ds^2 = -f(r)\mathrm{d}t^2 + \frac{1}{f(r)}\mathrm{d}r^2 + r^2\mathrm{d}\theta^2 + r^2\sin^2\theta\mathrm{d}\phi^2 \tag{2.5}$$

where, A_μ is the electromagnetic four-potential and

$$f(r) = \left(1 + \frac{r^2}{b^2} - \frac{2M}{r} + \frac{q_E^2 + q_M^2}{r^2}\right). \tag{2.6}$$

q_E, q_M and M are the integration constants, identified as electric charge, magnetic charge and mass of the black hole respectively. r_+, the horizon of the black hole is given by

$$f(r_+) = \left(1 + \frac{r_+^2}{b^2} - \frac{2M}{r_+} + \frac{q_E^2 + q_M^2}{r_+^2}\right) = 0. \tag{2.7}$$

We shall work in an ensemble where the asymptotic value of A_t is constant, which implies electric potential Φ_E defined as

$$\Phi_E = \frac{q_E}{r_+} \tag{2.8}$$

is constant in our thermodynamic analysis.

The Hawking Temperature of this Black Hole is given by

$$T = \frac{1}{\beta} = \frac{1}{4\pi r_+}\left[1 + \frac{3r_+^2}{b^2} - \Phi_E^2 - \frac{q_M^2}{r_+^2}\right]. \tag{2.9}$$

2.1 Holographic dictionary

$(3+1)$ dimensional dyonic black hole in asymptotically AdS spacetime is conjectured to be dual to a $(2+1)$ dimensional CFT living on the boundary of the AdS space, which has topology $R \times S^2$. The bulk gauge field is dual to a global $U(1)$ current operator J_μ. The CFT has a conserved global charge $\langle J^t \rangle$ given by

$$\begin{aligned} \langle J^t \rangle &= \frac{q_E}{16\pi G_4} \\ &= \frac{\sqrt{2}N^{3/2}q_E}{24\pi b^2} \end{aligned} \tag{2.10}$$

where, we use the holographic dictionary

$$\frac{1}{16\pi G_4} = \frac{\sqrt{2}N^{3/2}}{24\pi b^2}, \quad N \text{ is the degree of the gauge group of the } CFT.$$

The boundary CFT also has a constant magnetic field. The strength of the magnetic field is given by $B = q_M/b^2$ which can be read off from the asymptotic value of bulk field strength obtained from equation (2.4). We shall study the magnetic properties of this strongly coupled system using the holographic setup.

In section 5, we see that the CFT undergoes a phase transition. A system in the finite volume, in general, does not exhibit any phase transition. But in the large N limit, *i.e.*, when the number of degrees of freedom goes to infinity then it is possible to have a phase transition even in finite volume.

3. Thermodynamics of dyonic black hole

In our discussion of thermodynamics of dyonic black hole[2] we identify the cosmological constant $\Lambda = -6/b^2$ with the thermodynamic pressure of the system. In most treatments of black hole thermodynamics in AdS space, the cosmological constant is treated as a constant parameter, *i.e.* thermodynamics and phase structure of black holes are studied in a fixed AdS background. In [13], the authors first considered the cosmological constant as a dynamical variable of the system. Later it was suggested in [14, 15, 16, 17, 18, 19] that Λ can be treated as a thermodynamic variable of the system. In fact, in presence of

[2]For thermodynamics of dyonic-dilaton black hole look at [12].

a cosmological constant the first law of black hole thermodynamics becomes inconsistent with the Smarr relation (the scaling argument is no longer valid) unless the variation of Λ is included in the first law [10]. In [10] it has also been shown that once we consider variation of Λ in the first law, the black hole mass M is then identified with enthalpy rather than internal energy of the system. Therefore, in the following discussion we take,

$$P = -\frac{\Lambda}{8\pi} = \frac{3}{8\pi}\frac{1}{b^2}. \tag{3.1}$$

Thus our ensemble is characterised by T, P, q_M and Φ_E. The corresponding free energy W is given by

$$W = E - TS - \Phi_E q_E. \tag{3.2}$$

3.1 On-shell action and background

We discuss the thermodynamics of black holes in the Euclidean framework as generally prescribed by Gibbons and Hawking. The canonical partition function is defined by a functional integral over metrics with the Euclidean time coordinate τ identified with period β.

$$\mathcal{Z} = \int [\mathcal{D}g] \mathrm{e}^{-I_E}, \tag{3.3}$$

I_E is the Euclidean action. In the semi-classical limit that we are considering, the dominant contribution to the path integral comes from classical solutions to the equations of motion. In this case,

$$\log \mathcal{Z} = -I_E^{onshell}, \tag{3.4}$$

where $I_E^{onshell}$ is the action evaluated on equations of motion. Using (2.2, 2.3) we can write

$$I_E^{onshell} = \frac{1}{16\pi G_4} \int \mathrm{d}^4x \sqrt{g} \left(F^2 + \frac{6}{b^2} \right). \tag{3.5}$$

Free energy is thus given by:

$$W = -\frac{1}{\beta} \ln \mathcal{Z} = \frac{I_{onshell}}{\beta}. \tag{3.6}$$

The on-shell action is divergent because the r integration ranges from r_+ to ∞. Therefore, we need to regularize the action by introducing a finite cutoff $\tilde{R}$. Then, to renormalize the action, we can either add some counter-term to the original action or we can subtract the contribution of a background spacetime. Here we follow the first prescription. Method of background subtraction is discussed in appendix A.

For a electromagnetically charged black hole with mass M, magnetic charge q_M and electric potential at infinity Φ_E, the regularised on-shell action is given by

$$\begin{aligned} I_{BH} &= \frac{1}{16\pi G_4}\int_{r_+}^{\tilde{R}} d^4x\sqrt{g}\left(F^2+\frac{6}{b^2}\right) \\ &= \frac{\beta}{4G_4}\left[\frac{2(\Phi_E^2 r_+^2-q_M^2)}{\tilde{R}}+\frac{6\tilde{R}^3}{3b^2}-\frac{2(\Phi_E^2 r_+^2-q_M^2)}{r_+}-\frac{6r_+^3}{3b^2}\right]. \end{aligned} \tag{3.7}$$

Here $\tilde{R}$ is the cutoff. We shall take $\tilde{R}\to\infty$ at the end. β is the period of Euclidean time coordinate τ, identified as inverse Hawking temperature

$$\beta = \frac{4\pi}{f'(r_+)} = \frac{4\pi b^2 r_+}{3r_+^2+b^2\left(1-\Phi_E^2-\frac{q_M^2}{r_+^2}\right)}. \tag{3.8}$$

Note that the second term in equation (3.7) gives a diverging contribution to free energy as $\tilde{R}\to\infty$. To tame the divergence we add counterterms following [20]. We find that the on-shell action can be made finite with the following counterterms,

$$S_{ct} = \frac{1}{8\pi G_4}\int_{\partial\mathcal{M}} d^3x\sqrt{-\gamma}\left(c_1+c_2R^{(3)}\right). \tag{3.9}$$

Here $\partial\mathcal{M}$ is the asymptotic boundary of AdS spacetime, γ is the induced metric on the boundary, $R^{(3)}$ is the Ricci scalar calculated for the metric γ. c_1 and c_2 are two numerical constants, their values are given by,

$$c_1 = -\frac{1}{b}, \qquad c_2 = \frac{b}{4}. \tag{3.10}$$

Hence, the free energy is given by,

$$W = \frac{I}{\beta} = \frac{1}{4G_4}\left[-\Phi_E^2 r_+ + \frac{3q_M^2}{r_+} - \frac{8\pi P r_+^3}{3} + r_+\right]. \tag{3.11}$$

3.2 Thermodynamic variables and their relations

Using the expression for free energy $W(T,\Phi_E,q_M,P)$ in equation (3.11), all the thermodynamical variables can be computed easily. We quote the results as follows:

$$\begin{aligned} q_E &= -\frac{\partial W}{\partial\Phi_E} = \frac{\Phi_E r_+}{G_4}; \\ \Phi_M &= \frac{\partial W}{\partial q_M} = \frac{q_M}{G_4\, r_+}; \\ S &= -\frac{\partial W}{\partial T} = \beta^2\frac{\partial W}{\partial\beta} = \frac{1}{4G_4}4\pi r_+^2 = \frac{A_H}{4G_4}; \\ V &= \frac{\partial W}{\partial P} = \frac{4\pi}{3}r_+^3. \end{aligned} \tag{3.12}$$

Here Φ_M is the chemical potential corresponding to magnetic charge q_M. Using equation (3.2) we can calculate the enthalpy E of the BH given by:

$$E = W + TS + \Phi_E q_E = \frac{M}{G_4}. \tag{3.13}$$

Thus we see that enthalpy E is equal to the mass of the black hole. From now and onwards, we set $G_4 = 1$.

3.3 Equation of state

In [8] it has been argued that once we consider the cosmological constant as thermodynamic pressure and the volume covered by the event horizon as thermodynamic volume, the black hole equation of state has surprising similarity with equation of state of a Van der Waals fluid, which describes the liquid-gas phase transition qualitatively. One can write the pressure as a function of T, r_+, Φ_E and q_M as follows from equation (2.9):

$$P = \frac{T}{v} - \frac{1 - \Phi_E^2}{2\pi v^2} + \frac{2q_M^2}{\pi v^4} \tag{3.14}$$

where, $v = 2r_+$ can be identified with the specific volume of the system [8]. This equation describes different phases of a dyonic black hole in a fixed electric potential and magnetic charge ensemble which is similar to extended liquid-gas phase diagram. We shall discuss the phase structure in section 4.

3.4 Specific heats and thermodynamic stability

In thermodynamics, heat capacity or thermal capacity is an important measurable physical quantity. It specifies the amount of heat required to change the temperature of an object or body by a given amount. There are two different heat capacities associated with a system. C_V : measures the heat capacity when the heat is added to the system keeping the volume constant and C_P : when the heat is added at constant pressure. Heat capacities can be calculated using the standard thermodynamic relations:

$$C_V = T\frac{\partial S}{\partial T}\bigg|_V, \qquad C_P = T\frac{\partial S}{\partial T}\bigg|_P. \tag{3.15}$$

Using the expression for black hole entropy (equation 3.12) one can calculate the heat capacities:

$$S = \frac{A_H}{4} = \pi r_+^2 = \pi\left(\frac{3V}{4\pi}\right)^{2/3} \quad \Rightarrow C_V = 0. \tag{3.16}$$

Using equation (3.14) C_P is given by

$$C_P = 2S\left[\frac{8PS^2 + S(1-\Phi_E^2) - \pi q_M^2}{8PS^2 - S(1-\Phi_E^2) + 3\pi q_M^2}\right]. \tag{3.17}$$

Thermodynamic stability requires that $C_P > 0$. This implies the stability of different thermodynamic phases are bounded by,

$$\frac{1}{3}S(1-\Phi_E^2) - \frac{8}{3}PS^2 < \pi q_M^2 < 8PS^2 + S(1-\Phi_E^2). \tag{3.18}$$

We shall get back to this point in section 6.

The specific heat C_P diverges when the denominator vanishes. We shall discuss this issue in section 4.2 when we discuss about the critical points in black hole phase diagram.

4. Black hole phase transition

$P-V$ diagram for a Van der Waals fluid shows multiple volume solutions (gas, liquid and a thermodynamically unstable state) for a given pressure in a specific range. The presence of the unstable state is unphysical because $\partial P/\partial V|_T$ is positive for this state. This problem is avoided by Maxwell's equal area law to give the corrected $P-V$ diagram, which indirectly states that the system will exist in a phase which has the minimum value of corresponding free energy. When the free energy of gas and liquid phases crosses each other, the system instantaneously jumps from the higher free energy phase to the lower. When the two free energies are equal however, the gas and liquid phases coexist.

An exactly similar behaviour is observed when we study the equation of state of a dyonic black hole. Van der Waals equation and black hole's equation of state are different in nature. The first one is a cubic equation whereas the second one is quartic. Therefore, black hole's equation should have four roots (for v) for a given set of parameters. However, it turns out that there exists *maximum* three real positive solutions for v (the fourth root is negative in this case). In this section we study the phase diagram of dyonic black hole. We find that there is a phase transition between a small black hole and large black hole which is analogous to the liquid-gas phase transition. We also discuss the limit of this phase transition as $q_M \to 0$ and show that it reduces to the Hawking-Page phase transition [21].

4.1 Different phases of black holes

We write P as a function of thermodynamic volume V from equation (3.14)

$$P = \frac{T}{V^{1/3}}\left(\frac{\pi}{6}\right)^{1/3} - \frac{1-\Phi_E^2}{2\pi V^{2/3}}\left(\frac{\pi}{6}\right)^{2/3} + \frac{2q_M^2}{\pi V^{4/3}}\left(\frac{\pi}{6}\right)^{4/3}. \tag{4.1}$$

The $P-V$ plot (figure 3a) we get keeping T, Φ_E and q_M fixed, are identical to that of liquid-gas case in Van der Waals case. In figure (3b) we plot the same curves for varying T.

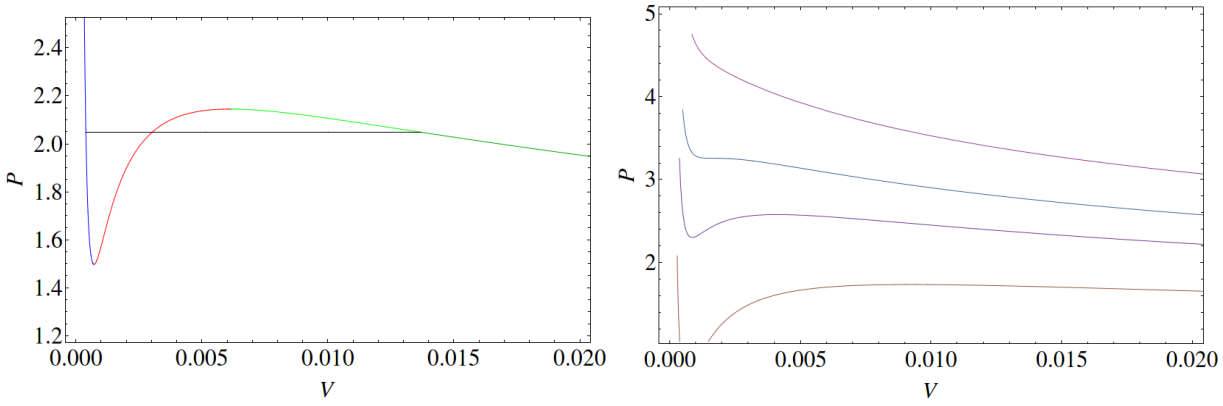

(a) **(b)**

Figure 3: **(a)** $P-V$ diagram for all other parameters held constant ($q_M = 0.028$, $\Phi_E = 0.35$, $T = 1.05$). The black line refers to the coexistence pressure. Blue, red and green parts of the curve corresponds to Branch-1,2,3 respectively. **(b)** $P-V$ diagram for fixed $q_M(= 0.028)$ and $\Phi_E(= 0.35)$ and varying T. The second curve from the top corresponds to the Critical Point.

In the first figure we see that for a particular value of P in a window, we have three different solutions for black hole horizon. These are identified as Branch-1 (Blue), Branch-2 (Red) and Branch-3 (Green) (figure 3a). For large P only Branch-1 (SBH) exists, while for low P Branch-3 (LBH) is the only solution. As we shall see later, Branch-2 always gives a thermodynamically unstable phase. The remarkable resemblance with the liquid-gas phase transition in Van der Waals case is clearly apparent here.

As we alter the Temperature (see figure 3b), we notice that above a critical temperature, Branch-2 totally disappears and Branch-1 and 3 coalesce. Below the critical temperature however, there exist 3 phases of black hole in a particular pressure window, out of which one is unstable.

Unlike Van der Waals equation, we have 2 more free parameters apart from T: q_M and Φ_E. As we vary q_M the behavior of $P-V$ diagram is quite similar to what we have seen for varying T (See figure 4a). Here also, there exists a critical magnetic charge $q_{M(c)}$ above which there exists only one branch of solution. Nucleation of other two branches starts at $q_{M(c)}$ (depending on the values of other parameters).

$q_M \to 0$ **limit:** We note an interesting and important behavior as $q_M \to 0$. Branch-1 overlaps with y-axis i.e. r_+ for small black hole approaches to zero in $q_M \to 0$ limit. Thus the small black hole solution evaporates to a global AdS, which exists for all values of pressure. However, the other two branches still persist in this limit.

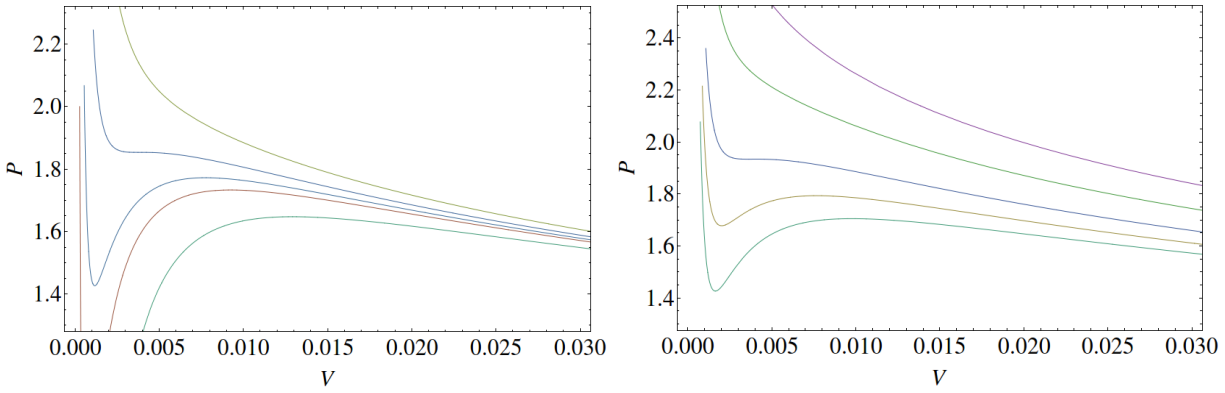

(a) **(b)**

Figure 4: **(a)** $P-V$ diagram for fix $T(=0.96)$ and $\Phi_E(=0.35)$ and varying q_M. The last curve corresponds to $q_M = 0$. **(b)** $P-V$ diagram for fix $q_M(=0.038)$ and $T(\approx 1)$ and varying Φ_E. The last curve corresponds to $\Phi_E = 0$.

Finally, we vary Φ_E keeping T and q_M fixed (figure 4b). From the equation of state we can easily check that if $\Phi_E^2 > 1$ then there exists only one branch for any values of T and q_M. Criticality starts at $\Phi_E^2 = 1$ and persists for $0 < \Phi_E^2 < 1$. At $\Phi_E = 0$, which is a purely magnetically charged system, the phase diagram is similar[3] to electrically charged black hole in fixed charge ensemble of [7, 8].

[3]Since the metric (2.6) is symmetric in electric and magnetic charges, pure constant electric charge system behaves similar to the pure constant magnetic charge ensemble.

4.2 Critical points

Studying the figure (3b), (4a) and (4b) in the last section we see that there exists a critical hyper-surface in the parameter space (T, Φ_E and q_M) where Branch-1 and 3 coalesce and Branch-2 vanishes. If we go beyond that hyper-surface we have only one branch and below that hyper-surface we have three different branches which is much alike the critical point in liquid-gas phase transitions. But the difference is, in case of liquid-gas phase diagram the critical point was determined by the temperature only, whereas in this case it is a two dimensional hyper-surface. The critical surface can be obtained in the following way.

For multiple phases to occur in our system, we need a region of positive slope in $P - V$ diagram. Using equation (3.14) we thus have the bound:

$$-\frac{\pi}{2}v^5 P' = Tv^3 - \frac{1-\Phi_E^2}{\pi}v^2 + \frac{8q_M^2}{\pi} < 0. \tag{4.2}$$

Real positive solution for v is possible when

$$|\Phi_E| < 1 \quad \text{and} \quad (1-\Phi_E^2)^3 - 54\pi^2 q_M^2 T^2 \geq 0. \tag{4.3}$$

The equality holds at the critical point where Branch-2 just vanishes, giving us the equation for the critical surface:

$$3\sqrt{6}\pi q_{M(c)} T_c = (1-\Phi_{E(c)}^2)^{3/2}. \tag{4.4}$$

Using the equation of state we find the expression for critical pressure and volume as

$$P_c = \frac{9\pi T_c^2}{16\left(1-\Phi_{E(c)}^2\right)}, \qquad v_c = \frac{2\sqrt{6}q_{M(c)}}{\left(1-\Phi_{E(c)}^2\right)^{1/2}}. \tag{4.5}$$

The relations (4.4) and (4.5) can also be reached directly by demanding divergence of C_P in equation (3.17). This designates the boundary of multiple-phase regime.

4.2.1 Critical exponents

On the critical surface given by equation (4.4) and (4.5), we calculate the ratio of critical pressure times critical volume over critical temperature. The result is given by

$$\frac{P_c v_c}{T_c} = \frac{3}{8}, \tag{4.6}$$

which is a universal constant and is exactly the same as for the Van der Waals fluid. Defining new reduced variables

$$p_R = \frac{P}{P_c} \qquad t_R = \frac{T}{T_c} \qquad v_R = \frac{v}{v_c}, \tag{4.7}$$

equation of state (equation 3.14) can be written as (which has the same form as in [8])

$$8t_R = 3v_R \left(p_R + \frac{2}{v_R^2} \right) - \frac{1}{v_R^3}. \tag{4.8}$$

We also calculate the critical exponents defined as,

$$\begin{aligned} \text{Specific heat}: &\quad C \sim |T - T_c|^{-\alpha} \\ \text{order parameter}: &\quad \mathcal{O} \sim |T - T_c|^{\beta} \\ \text{susceptibility or compressibility}: &\quad \chi(\text{or } \kappa) \sim |T - T_c|^{-\gamma} \\ \text{equation of state}: &\quad (p - p_c) \sim (v - v_c)^{\delta}. \end{aligned} \tag{4.9}$$

In this case the order parameter is given by the difference between the radii of large and small black hole ($|r_+^L - r_+^S|$). Calculation of these critical exponents is fairly straight forward. Our final results are given by,

$$\alpha = 0, \qquad \beta = \frac{1}{2}, \qquad \gamma = 1, \qquad \delta = 3. \tag{4.10}$$

Note that these results match with mean-field theory.

4.3 Phase transition

In order to study phase transition we look at the free energy as a function of temperature for constant P, q_M and Φ_E. For better understanding, we use different colors for three different branches that appear in P-V diagram. In figure (5a), the blue, red and green lines are the free energies for small, unstable and large black hole as a function of temperature (same as in figure 3a). From this plot it is clear that at low temperature there exists only one branch. As we increase temperature two new branches appear (the upper cusp) at $T = T_c$ (black hole nucleation temperature). At this temperature the free energies of two new branches are greater than the first one, hence the first branch dominates the thermodynamics. Upon further increase of temperature, we see that at some temperature ($T = T_o$) the green curve crosses the blue one and after that the free energy of the large

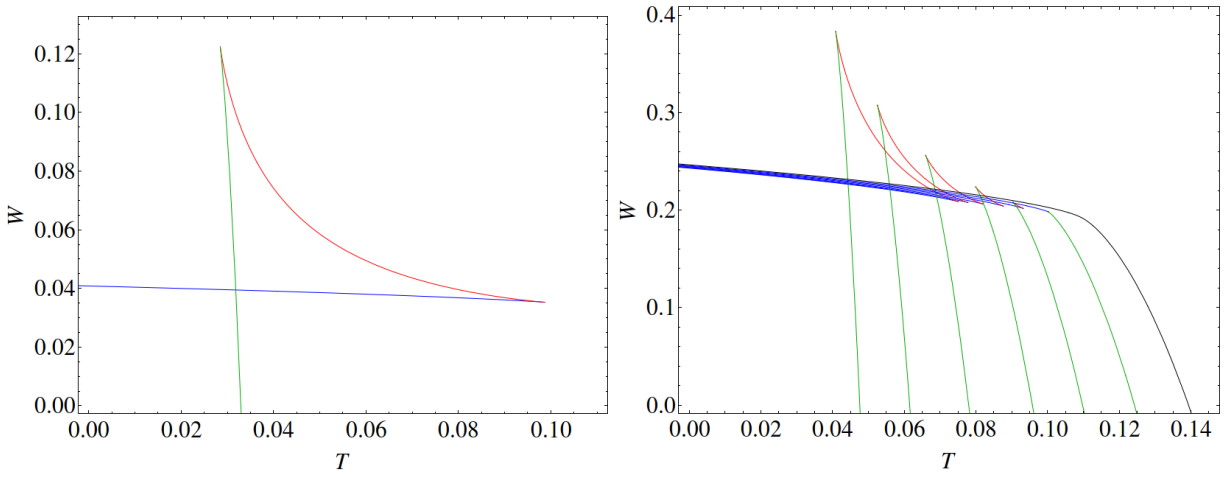

(a) **(b)**

Figure 5: **(a)** $W - T$ plot for all other parameters fixed ($P = 0.0035$, $\Phi_E = 0.8$, $q_M = 0.068$). The graph has three separate branches: Branch-1 (Blue), Branch-2 (Red) and Branch-3 (Green). **(b)** $W - T$ diagram for fixed $\Phi_E = 0.5$, $q_M = 0.28$ and varying P. $P \approx 0.018$ is the critical point in this case, after which only one solution of BH remains (the black curve).

black hole dominates over the other two branches. This implies a phase transition between small black hole and large black hole at T_o. There exists a temperature $T_A > T_o$, where Branch-1 and 2 vanishes, is called annihilation temperature (T_A).

The unstable black hole (branch-2, the red curve in the figure 5a) is always thermodynamically disfavored as the free energy of this branch is greater than the free energy of the other two branches for any temperature. Branch-1 and Branch-3 intersects at the coexistence point T_o (≈ 0.03) which is similar to liquid gas phase transition.

The coexistence point can be reached easily by demanding free energy (W) to be same for two different volumes: $V_1(r_+^{(1)})$ and $V_2(r_+^{(2)})$ which are the roots of equation (4.1) for some P, T, q_M, Φ_E such that $P'(V) < 0$. As we vary the temperature, black hole never goes to Branch-2 phase, but jumps from Branch-1 to branch-3 directly at the coexistence point. Therefore, we correct the $P - V$ diagram by replacing the oscillating part by a flat line (See figure 3a). The flat line can be obtained at some particular pressure called coexistence pressure P_{co} where the free energy W of both the phases (1 and 3) are same. This is the Maxwell construction. Needless to mention, the coexistence pressure depends on the temperature (also on other two parameters in this case q_M and Φ_E). In figure (6a) we plot coexistence pressure vs. temperature for different values of Φ_E. Coexistence

points form a plane in $T - P - \Phi_E$ plane (keeping q_M fixed).

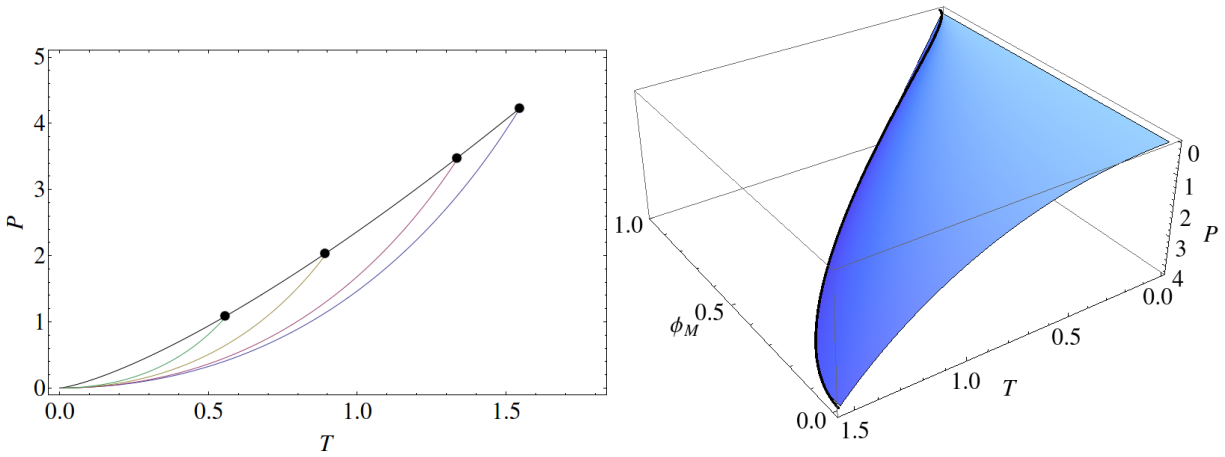

(a) **(b)**

Figure 6: **(a)** Colored curves are the Coexistence Curves in $P - T$ phase space for different values of Φ_E. The rightmost is for the lowest value of Φ_E which is 0. The black curve is however the critical curve for arbitrary Φ_E. **(b)** Coexistence Plane in $P - T - \Phi_E$ phase space. Above the plane lies the Small BH, while below the plane we have Large BH. The Black Graph is the Critical Curve.

4.3.1 Hawking-Page phase transition

In figure (7) we plot free energy vs. temperature for different values of q_M, keeping Φ_M fixed. In this section we investigate the $q_M \to 0$ limit carefully. From the plot it is clear that for large q_M we can not see any phase transition (the topmost plot). There exists only one stable black hole. At $q_M = q_{M(c)}$ two new branches appear one of them is unstable. As we further decrease $q_M(> 0)$ the $W - T$ plot is same as in figure (5a), what we have already discussed. Here we discuss the $q_M \to 0$ limit of these plots (the bottom most curve). In this limit we see that the blue line (corresponding to small black hole) overlaps with x-axis. This implies that the free energy of the small black hole, in this particular limit, reduces to zero. That is, the small black hole reduces to a global AdS spacetime (the size of this black hole also reduces to zero in this limit, as we have discussed in section 4.1). Hence, the LBH - SBH phase transition reduces to Hawking-Page phase transition (a transition between black hole and a global AdS spacetime).

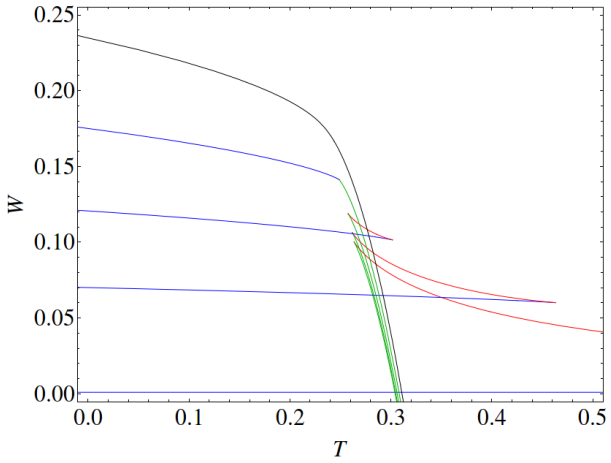

Figure 7: W vs. T for fixed $P = 0.12$, $\Phi_E = 0.045$ and varying q_M. Criticality occurs at $q_M = 0.173$. The bottommost graph is for $q_M = 0$.

An important point to note here is that, in $q_M \to 0$ limit r_+ also goes to zero but the ratio q_M/r_+ remains fixed (which we call Φ_M). Therefore, the global AdS spacetime has a constant Φ_M. Since we are working in a constant Φ_E ensemble, the global AdS space has a constant electric potential as well.

This completes our discussion on black hole phase transition in presence of an arbitrary magnetic charge. We have established the resemblance of Small-Large black hole phase transitions in asymptotically AdS space (in constant electric potential and magnetic charge ensemble) with the liquid-gas phase transition.

4.3.2 Planar black hole

Planar black holes have horizon topology $R \times R^2$. Black holes with R^2 horizon topology (space part only) can arise in asymptotically AdS space. These black hole are also called *Ricci flat* black holes. In our analysis, if we consider the black hole mass (or r_+) to be very large, all the equations and expressions reduces to those of planar black hole.

Phase diagram for planar black hole does not show any kind of criticality. For any value of Φ_E and q_M there exists only one branch for any temperature. This is clear from the equation of state for planer black hole,

$$P = \frac{T}{v} + \frac{\Phi_E^2}{2\pi v^2} + \frac{2q_M^2}{\pi v^4}. \tag{4.11}$$

Because of the *Ricci flat* horizon topology planar black hole is always thermodynamically stable for any temperature. However, planar black hole with toroidal horizon topology undergoes a phase transition from black hole to AdS soliton phase [22, 23]. It would be interesting to check if magnetic charge has any nontrivial effect on this phase transition.

5. Magnetic properties of boundary CFT

We have discussed in section 2.1 that the boundary CFT has a constant magnetic field due to presence of a magnetic charge in the bulk spacetime. The magnetic field is given by,

$$B = \frac{q_M}{b^2}. \tag{5.1}$$

When we consider thermodynamics of the boundary theory we define a variable $\mathcal{M}$ (magnetization), conjugate to the external magnetic field B. Different phases of boundary theory are also characterised by this new variable $\mathcal{M}$ defined by the following relation[4],

$$\mathcal{M} = -\frac{\partial W}{\partial B}\bigg|_T. \tag{5.2}$$

Using the expression (3.11) for W we find,

$$\mathcal{M} = -\frac{\partial W}{\partial B}\bigg|_T = -b^2\left(\frac{q_M}{r_+}\right). \tag{5.3}$$

It is worth to note that the positive definiteness of r_+ implies $\mathcal{M}$ and B always have opposite sign.

We calculate free energy and temperature of the CFT in terms of B and $\mathcal{M}$ (boundary parameters) to study the phase structure of the system,

$$W = \frac{1}{4}\left[-(1-\Phi_E^2)b^4\frac{B}{\mathcal{M}} - 3B\mathcal{M} + b^{10}\frac{B^3}{\mathcal{M}^3}\right], \tag{5.4}$$

$$T = \frac{1}{\beta} = \frac{1}{4\pi}\left[-(1-\Phi_E^2)\frac{1}{b^4}\frac{\mathcal{M}}{B} - 3b^2\frac{B}{\mathcal{M}} + \frac{1}{b^8}\frac{\mathcal{M}^3}{B}\right]. \tag{5.5}$$

[4]Since we are studying the thermodynamic properties of a boundary theory in the context of the AdS/CFT we keep the radius of the AdS space to be constant.

5.1 Magnetization of boundary phases

In this section we discuss different phases of the boundary CFT dual to different black hole phases. W in equation (5.4) can be plotted against T for varying B. Since B is proportional to q_M, the plot is the same as in figure (7).

For B above a critical value B_c (which is proportional to $q_{M(c)}$, discussed in Section 4.1) there exists only one phase of boundary CFT and magnetization of this phase is a continuous function of temperature. As B goes below B_c the boundary theory develops two more new phases. Therefore, in this case the theory has three different phases (in a given temperature window). See figure (8).

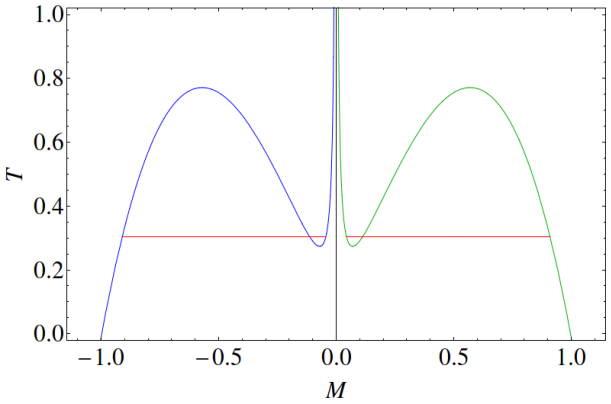

Figure 8: $T - \mathcal{M}$ plot and Maxwell's construction. Red line is the co-existence point (corresponds to temperature T_0).

The blue (green) curve in figure (8) corresponds to positive (negative) magnetic field. In this figure we see that, below a critical temperature there exists only one phase with high magnetization (dual to small black hole). Above the critical temperature, there are three possible phases with different magnetization. Among them the middle one is thermodynamically unstable. The phase with small magnetization correspond to the large black hole phase in the dual theory. The red line indicates the transition temperature T_o. Above this temperature, thermodynamics is dominated by the phase with small magnetization. Therefore a sharp jump in magnetization is observed at the transition temperature. Later in section 5.2, we discuss about this transition in detail. In figure (1) we plot the same graph removing the unstable branch using Maxwell's construction. $\mathcal{M}$ vs. T plots for different values of magnetic field and B vs. $\mathcal{M}$ plots for different values of temperature are discussed in Appendix B.

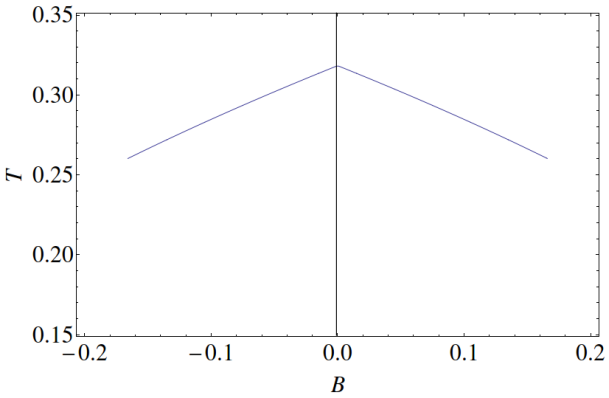

Figure 9: T_0 vs. B curve (for $\Phi_E = 0.8$). The end point is the critical point (for a fixed Φ_E). Above (below) the line small (large) magnetization black hole dominates the thermodynamics.

The transition temperature T_o depends on the external magnetic field. As we increase the magnetic field from 0 up to B_c the transition temperature decreases (figure 9). For $B > B_c$ there exists only one stable branch.

5.1.1 $B \to 0$ limit: Ferromagnetic like behaviour

$B \to 0$ limit, in particular is interesting. In this limit we see that the low temperature phase has a constant magnetization whereas the high temperature phase has zero magnetization. There is a transition between zero magnetization phase to constant magnetization phase as we decrease the temperature (See figure 1). Unlike ferromagnetic materials, here we find that the magnetization is discontinuous at the transition temperature. The constant magnetization phase is dual to global AdS phase in the bulk. As we have discussed before, in this limit the radius of small black hole goes to zero with q_M/r_+ fixed. In other words the small black hole evaporates to global AdS with constant Φ_E and $\mathcal{M}$. A more detailed discussion can be found in Appendix C.

As we have explained before, in the limit $B \to 0$ LBH/SBH phase transition reduces to Hawking-Page phase transition. Therefore, low temperature phase (dual to global AdS) of the boundary theory has zero free energy whereas the high temperature phase dual to LBH has free energy of order $N^{3/2}$ in the limit $N \to \infty$. This phase transition is identified with confinement-deconfinement phase transition of gauge theory [24]. Therefore, we see that the confined phase has a constant magnetization whereas the deconfined phase has zero magnetization.

5.2 Magnetic susceptibility of boundary theory

Depending on the Temperature and applied Magnetic Field, boundary theory shows either diamagnetic or paramagnetic behavior. To study the same we calculate magnetic susceptibility using the formula:

$$\chi = \left.\frac{\partial \mathcal{M}}{\partial B}\right|_T . \tag{5.6}$$

A system is said to be diamagnetic if $\chi < 0$ and paramagnetic if $\chi > 0$. The magnetic properties of a physical substance mainly depend on the electrons in the substance. The electrons are either free or bound to atoms. When we apply an external magnetic field these electrons react against that field. In general one can see two important effects. One, the electrons start moving in a quantised orbit in presence of the magnetic field. Two, the spins of the electrons tend to align parallel to the magnetic field. One can neglect the effect of atomic nuclei compared to these two effects, as they are much heavier than electrons. The orbital motion of electrons is responsible for diamagnetism whereas, alignment of electrons' spin along the magnetic field gives rise to paramagnetism. In a physical substance, these two effects compete. In diamagnetic material the first one (orbital motion) is stronger than the second one, and vice-versa in a paramagnetic material.

The temperature in (equation 5.5) can be written in the following differential form for a constant Φ_E:

$$\mathrm{d}T = \frac{\partial T}{\partial B}\mathrm{d}B + \frac{\partial T}{\partial \mathcal{M}}\mathrm{d}\mathcal{M}. \tag{5.7}$$

χ from this expression can be written as

$$\chi = \left.\frac{\mathrm{d}\mathcal{M}}{\mathrm{d}B}\right|_T = \frac{\partial T}{\partial B}\frac{\partial \mathcal{M}}{\partial T} = \frac{\mathcal{M}}{B}\left(\frac{3b^{10}B^2 + \mathcal{M}^4 - b^4\mathcal{M}^2\left(1-\Phi_E^2\right)}{3b^{10}B^2 + 3\mathcal{M}^4 - b^4\mathcal{M}^2\left(1-\Phi_E^2\right)}\right). \tag{5.8}$$

We plot χ against T for various B to study the magnetic behaviour of the system. Our results are as follows:

1. There exists a magnetic field $B^* > B_c$, above which the CFT is diamagnetic for all temperatures (see figure 2a).

2. For $B_c < B < B^*$, still the boundary theory has a single phase but this phase shows two crossovers between paramagnetic and diamagnetic phases. At high and low temperature the system behaves like a diamagnetic system, while in between it shows paramagnetic behavior. See figure (2b).

3. For $B < B_c$ (but still close to B_c), the unstable branch of BH pops up. Thus we see a phase transition at T_o from Small BH branch to Large BH branch, both of them being paramagnetic. As temperature is decreased (increased), Small BH (Large BH) branch crosses over to a diamagnetic phase. Figure (10) shows the segment of the curves near $T = T_o$.

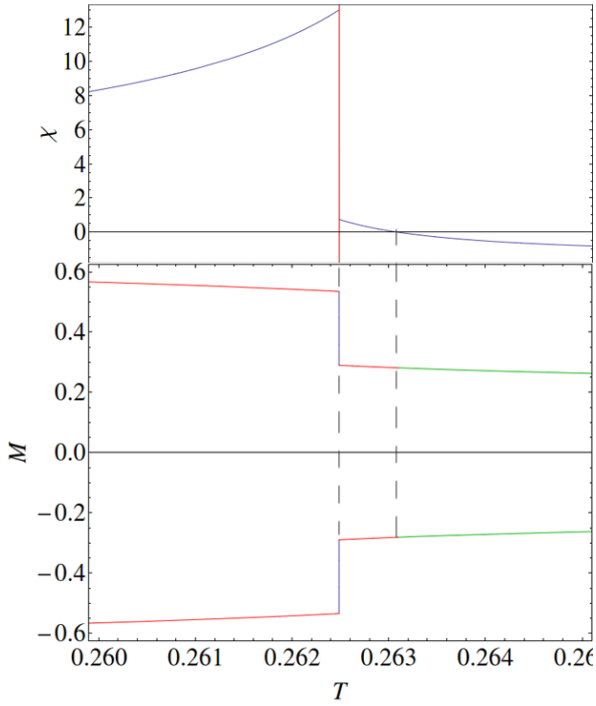

Figure 10: $\mathcal{M}$ vs. T and corresponding χ vs. T for $B < B_c$ (but close to it). In this plot it is observed that small magnetization branch has $\chi > 0$ for temperature close to the transition temperature. As we increase temperature, it crosses over to diamagnetic phase $\chi < 0$. Similarly, low temperature phase near the transition temperature hase $\chi > 0$ but as temperature is decreased its susceptibility becomes negative (the plot does not show the low temperature behaviour.)

4. Below B_c, when magnetic field is even below a certain value $B^{\#}$ (discussed in Appendix D), the paramagnetic branch of Large BH gets cut off in the Maxwells' construction (figure 2c). Thus the phase transition occurs from paramagnetic Small BH to diamagnetic Large BH.

5.2.1 High temperature behavior of magnetic susceptibility

In the high temperature limit, as we know that only the small magnetization solu-

tion (Large BH) dominates, temperature (equation 5.5) has the leading contribution from:

$$T \approx -\frac{3B}{4\pi\mathcal{M}} \tag{5.9}$$

and χ for large T will thus be given by:

$$\chi \approx \frac{\mathcal{M}}{B} \approx \left(-\frac{3}{4\pi}\right)\frac{1}{T}. \tag{5.10}$$

Hence we see that the Curie's Law is satisfied with a negative Curie Constant $-3/4\pi$.

6. Stability analysis

We conclude our discussion by analysing the stability of black hole solutions. When entropy S is a smooth function of extensive variables x_i's then sub-additivity of entropy is equivalent to the Hessian matrix $\left[\frac{\partial^2 S}{\partial x_i \partial x_j}\right]$ being negative definite. For canonical ensemble the only extensive variable is mass (or energy), therefore, sub-additivity of entropy implies that $C_P > 0$. For grand canonical ensemble, the variables are mass and charges therefore the stability lines are determined by finding the zeros of the determinant of the Hessian matrix. It has been argued in [25] that the zeros of the determinant of the Hessian of S with respect to M and q_i's coincide with the zeros of the determinant of the Hessian of the Gibbs (Euclidean) action,

$$I_G = \beta\left(M - \sum_i q_i^{\text{phys}}\Phi_i\right) - S \tag{6.1}$$

with respective to r_+ and q_i's keeping β and Φ_i's fixed. Note that q_i's are the charge parameters entering into the black hole solutions where q_i^{phys}'s are the physical charges. Though this criteria can figure out the instability line in the phase diagram but it is unable to tell which sides of the phase transition lines correspond to local stability. One can figure out the stability region by knowing the fact that zero chemical potential and high temperature must correspond to a stable black hole solution.

We compute the zeroes of the Hessian of free energy $W = M - \Phi_E q_E - TS$ with respect to q_E and r_+ keeping T and Φ_E fixed, which gives us one condition (or bound) on the phase space. Positivity of temperature will give another condition. These two conditions

give the following bound on the phase space.

$$3q_M^2 + \frac{3r_+^4}{b^2} - r_+^2(1-\Phi_E^2) > 0, \qquad -q_M^2 + \frac{3r_+^4}{b^2} + r_+^2(1-\Phi_E^2) > 0. \tag{6.2}$$

These are the same conditions we obtained by arguing positivity of specific heat of the system (equation 3.18). These conditions can also be obtained from the relation (4.2): $P'(r_+) < 0$, which is true for two solutions - SBH and LBH. In figure (11) and (12) We plot these stability lines and find that all values of q_M, Φ_E and $T > 0$ results in a stable solution.

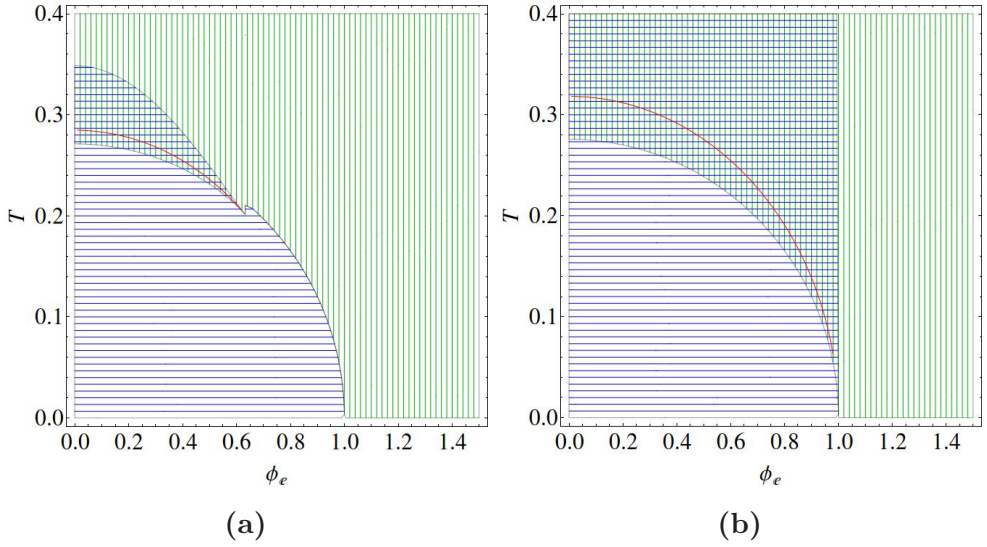

Figure 11: Stability plots in $T - \Phi_E$ phase space for **(a)** $q_M < q_{M(c)}$ and **(b)** $q_M = 0$. Horizontal blue lines correspond to Small BH solution stability region, whereas vertical green lines correspond to the stability region of Large BH. Red line corresponds to the phase transition.

7. Concluding remarks

In the paper we have studied the phase diagram of dyonic black hole in constant electric potential ensemble. An important thing to note here is that the equation of state (3.14) does not contain the global AdS spacetime as a solution. The equation of state has two stable solutions (SBH and LBH) and we find there is a first order phase transition between them. However, when we take $q_M \to 0$ limit, the SBH evaporates to global AdS and the SBH-LBH phase transition boils down to usual Hawking-Page phase transition. Since we

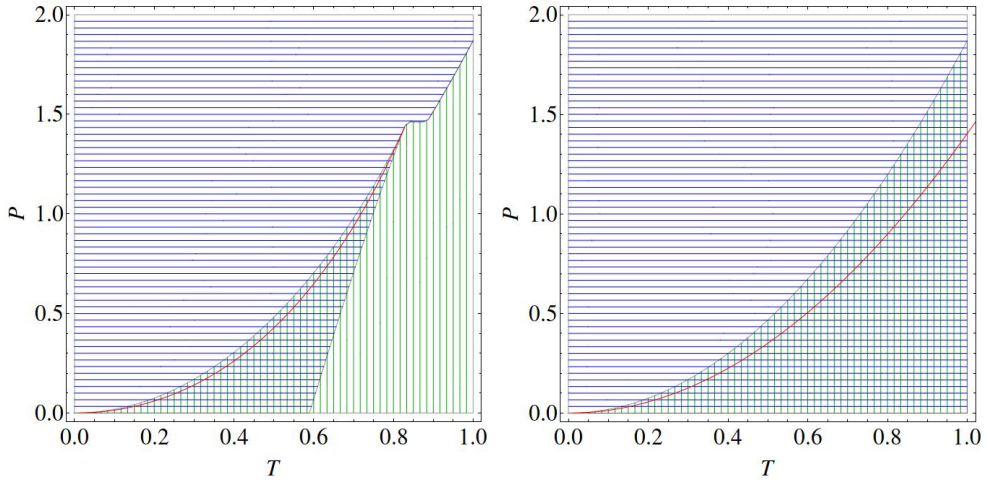

Figure 12: Stability plots in $P-T$ phase space for **(a)** $q_M < q_{M(c)}$ and **(b)** $q_M = 0$. Horizontal blue lines correspond to Small BH solution stability region, whereas vertical green lines correspond to the stability region of Large BH. Red line corresponds to the phase transition.

keep the electric chemical potential constant the transition temperature depends on the value of Φ_E [27].

Our observation in section 5 can be understood from the electro-magnetic (EM) duality in the bulk. Since the bulk spacetime is four dimensional, it admits an EM duality. The electric charge can be interpreted as a magnetic charge in a dual frame and vice versa. Therefore, our Φ_M in equation (3.12) can also be interpreted as Φ_E in the dual frame. Hence, one can also have the same plots as shown in figure (13a) and (13b) for $\Phi_E\ Vs.\ q_E$ or $\Phi_E\ Vs.\ T$ (see figure (14) of [8]).

In [26, 27] the authors discussed different phases of boundary CFT which are dual to different bulk solutions. They considered a unitary matrix model in the weak coupling side and showed that in the large N limit, there exists three different saddle points which correspond to small, large and unstable black holes in the bulk. The key point of their observation is that in the canonical ensemble, the fixed electric charge constraint contributes an additional logarithmic term $\log(TrUTrU^\dagger)$ involving the order parameter, to the gauge theory effective action. However, in our case, we have a constant magnetic field in the boundary theory. It is a good exercise to understand the effect of this constant magnetic field in the effective action of boundary theory.

Acknowledgements

We would like to thank Nabamita Banerjee, Umut Gursoy, Pratik Roy and Dibakar Roychowdhury for many helpful discussions. SD would like to acknowledge the hospitality of *Nikhef, Amsterdam* where part of this project was done. Finally we are also indebted to the people of India for their unconditional support towards research and development in basic science.

Appendix

A. Background subtraction

We calculate on-shell action by subtracting the contribution of an extremal magnetically charged black hole with magnetic charge q_M. The reason to choose this particular background depends on our choice of ensemble (see [7]). The extremal black solution is given by equation (2.4) and (2.5) with $q_E \to 0$

$$f_e(r) = \left(1 + \frac{r^2}{b^2} - \frac{2M_e}{r} + \frac{q_M^2}{r^2}\right). \tag{A.1}$$

We consider that the extremal black hole has a constant electric potential which is same as Φ_E of the black hole. The black hole has a horizon radius r_e, given by

$$f_e(r_e) = \left(1 + \frac{r_e^2}{b^2} - \frac{2M_e}{r_e} + \frac{q_M^2}{r_e^2}\right) = 0. \tag{A.2}$$

The extremality condition is given by

$$r_e^2 + \frac{3r_e^4}{b^2} = q_M^2. \tag{A.3}$$

Therefore, the on-shell action of background turns out to be

$$I_E = \frac{1}{16\pi}\int_{r_e}^{R} d^4x\sqrt{g}\left(F^2 + \frac{6}{b^2}\right) = \frac{\beta'}{4}\left[\frac{-2q_M^2}{R} + \frac{6R^3}{3b^2} - \frac{-2q_M 2}{r_e} - \frac{6r_e^3}{3b^2}\right] \tag{A.4}$$

where, β' is the radius of the Euclidean time circle of background. β' can be obtained by identifying the asymptotic boundary geometry of the black hole spacetime and extremal black hole spacetime

$$\beta\sqrt{g_{\tau\tau}} = \beta'\sqrt{g^e_{\tau\tau}}.$$

Thus, we get

$$\beta' = \beta\left(1 - \frac{(M - M_e)b^2}{R^3}\right). \tag{A.5}$$

Subtracting the contribution of extremal black hole on-shell action from that of black hole we finally get,

$$I_{onshell} = I_{BH} - I_E = \frac{\beta}{4}\left[-\Phi_E^2 r_+ + \frac{3q_M^2}{r_+} - \frac{r_+^3}{b^2} + r_+ - 4r_e - \frac{8r_e^3}{b^2}\right]. \tag{A.6}$$

Hence, the free energy is given by,

$$W = \frac{I}{\beta} = \frac{1}{4}\left[-\Phi_E^2 r_+ + \frac{3q_M^2}{r_+} - \frac{8\pi P r_+^3}{3} + r_+ - 4r_e - \frac{64\pi P r_e^3}{3}\right]. \tag{A.7}$$

This renormalization prescription tells us that all the thermodynamic quantities we measure (for example energy, volume, charges etc.) are with respect to an extremal magnetic black hole background.

Once we have free energy $W(T, \Phi_E, q_M, P)$ at hand, all the thermodynamical variables can be computed easily. We quote the results as follows:

$$\begin{aligned}
q_E &= -\frac{\partial W}{\partial \Phi_E} = \Phi_E r_+; \\
\Phi_M - \Phi_M^{(e)} &= \frac{\partial W}{\partial q_M} = \frac{q_M}{r_+} - \frac{q_M}{r_e}; \\
S &= -\frac{\partial W}{\partial T} = \beta^2 \frac{\partial W}{\partial \beta} = \frac{1}{4} 4\pi r_+^2 = \frac{A_H}{4}; \\
V - V_e. &= \frac{\partial W}{\partial P} = \frac{4\pi}{3} r_+^2 - \frac{4\pi}{3} r_e^2.
\end{aligned} \tag{A.8}$$

where Φ_M is the chemical potential corresponding to magnetic charge q_M. Note that, volume and magnetic potential is measured with respect to the extremal BH background. Using equation (3.2) we can calculate the enthalpy E of the BH given by:

$$E = W + TS + \Phi_E q_E = M - M_e. \tag{A.9}$$

B. Critical points and $\mathcal{M}$ vs. B plots

W in equation (5.4) can be plotted against T for varying B. Since B is identified with q_M, the plot is the same as figure (7). This time Branch-1 corresponds to high magnetization (Small black hole), and Branch-3 corresponds to low magnetization (Large black hole). We note the key points of Small-Large BH phase transition in this language:

Critical Curve is given by:

$$T_c = \frac{2}{\pi\sqrt{6}b}(1-\Phi_{E(c)}^2)^{1/2} \tag{B.1}$$

or correspondingly:

$$B_c = \pm\frac{1}{6b}(1-\Phi_{E(c)}^2) \tag{B.2}$$

while, Magnetization $\mathcal{M}$ at critical point(s) is given by:

$$\mathcal{M}_c = \mp\frac{b^2}{\sqrt{6}}(1-\Phi_{E(c)}^2)^{1/2}. \tag{B.3}$$

A thing to note here will be the Nucleation temperature, T_N. As $B \to 0$, T_N saturates

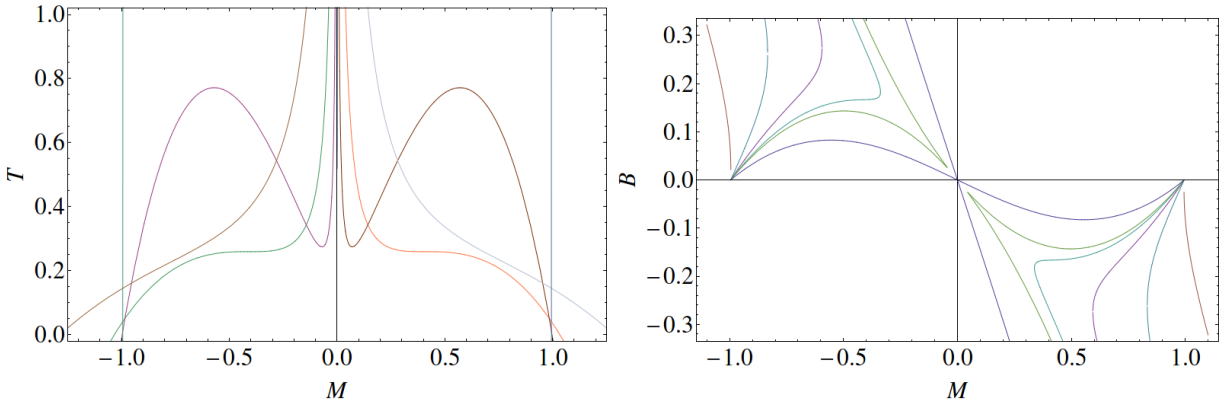

(a) **(b)**

Figure 13: **(a)** $T-\mathcal{M}$ graph for varying B ($\Phi_E = 0.1$). In order of the graphs near the T axis for small values of $\mathcal{M}$, the leftmost is for the highest positive B, and the rightmost for highest negative (magnitude) B. Criticality occurs in Green ($\mathcal{M} < 0$) and Light Orange ($\mathcal{M} > 0$) graphs ($B = \pm 0.165$). **(b)** $B-\mathcal{M}$ graph for varying T ($\Phi_E = 0.1$). In order of the graphs in the second quadrant, the leftmost is for the lowest T and the rightmost for highest T. Curves in the fourth quadrant are the segments of the same graphs. Criticality occurs at $T = 0.258$.

to some maximum value $T_{N(M)}$. Same is evident in figure (13b), (13a) ($T_{N(M)} \approx 0.3$).

It is the temperature when a curve (In figure 13a) touches the origin. At $T > T_{N(M)}$ (representative blue graph), $B = 0$ has 3 solutions. $T_{N(M)}$ will be given by the minima of $T - \mathcal{M}$ graph as $B \to 0$, which using equation 5.5 is:

$$T_{N(M)} = \frac{\sqrt{3}}{2\pi b}\sqrt{1 - \Phi_E^2}. \tag{B.4}$$

Similar to the nucleation temperature, coexistence temperature T_o also reaches its maximum value $T_{o(M)}$ as $B \to 0$. It can be easily found by finding root of W which gives:

$$T_{o(M)} = \frac{1}{\pi b}\sqrt{1 - \Phi_E^2}. \tag{B.5}$$

The coexistence point for the phase transition can also be translated similarly demanding W to be same for two phases, which will give corrected $B - \mathcal{M}$ and $T - \mathcal{M}$ plots. Coexistence curve (and plane) is however found to be like figure (14).

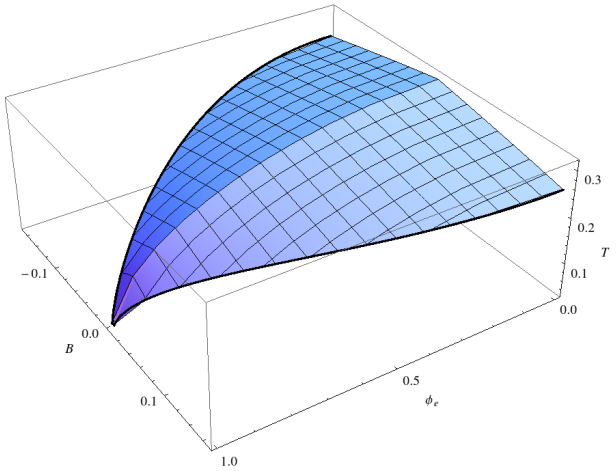

Figure 14: (b) Black Curve is the Critical Curve in $T - B - \Phi_E$ plane. The manifold is the coexistence plane. Above this plane lies the Small BH, and below it Large BH.

C. Magnetization from the minima of free energy

As we have seen that our system possesses a 'ferromagnetic' type behaviour in $B \to 0$ limit. In this appendix we investigate possible minima of the free energy as function of

temperature. We write the free energy from equation (3.2):

$$W = M - TS - \Phi_E q_E, \tag{C.1}$$

$$= -\frac{1}{2}\left(\frac{B}{\mathcal{M}}\right)(1-\Phi_E^2)b^4 - \frac{B\mathcal{M}}{2} - \frac{b^{10}}{2}\left(\frac{B}{\mathcal{M}}\right)^3 - \pi T b^8\left(\frac{B}{\mathcal{M}}\right)^2. \tag{C.2}$$

Using positive definiteness of r_+ we can write

$$W = \frac{1}{2}\left|\frac{B}{\mathcal{M}}\right|(1-\Phi_E^2)b^4 + \frac{|B\mathcal{M}|}{2} + \frac{b^{10}}{2}\left|\frac{B}{\mathcal{M}}\right|^3 - \pi T b^8\left|\frac{B}{\mathcal{M}}\right|^2. \tag{C.3}$$

$\partial W/\partial\mathcal{M} = 0$ will give us the back the equation of state (equation 5.5), and we will recover figure (13a) and (13b). To find the stable solutions of $\mathcal{M}$ in $B \to 0$ limit, we study the extremas of W using (C.2). For $r_+ = -b^4\frac{B}{\mathcal{M}}\Big|_{B\to 0} = 0$ we will have:

$$\mathcal{M} = \pm b^2\sqrt{(1-\Phi_E^2)}. \tag{C.4}$$

Whereas for $r_+ \neq 0$ the only solution is:

$$\mathcal{M} = 0 \quad \text{if} \quad T \geq T_{N(M)} = \frac{\sqrt{3}}{2\pi b}\sqrt{(1-\Phi_E^2)}. \tag{C.5}$$

First one is the background AdS solution which has some net finite magnetization even without any magnetic field. The second solution however corresponds to large black hole. The bound on the temperature is nothing but the maximum nucleation temperature (equation B.4), above which (for $B = 0$) there will always exist large black hole solution with radius

$$r_{+(LBH)} = \frac{2\pi b^2}{3}\left(T + \sqrt{T^2 - T_{N(M)}^2}\right). \tag{C.6}$$

To argue the dominance of the above solutions, we express W in the convenient form of r_+ in $B \to 0$.

$$W = \frac{r_+}{2b^4}\left[(1-\Phi_E^2)b^4 + \mathcal{M}^2 + b^2 r_+^2 - 2\pi T b^4 r_+\right]. \tag{C.7}$$

For AdS solution, $\mathcal{M} = \pm\sqrt{1-\Phi_E^2}$ and $r_+ = 0$, so the free energy vanishes. For the large black hole solution the free energy is given by

$$W_0 = \frac{1}{2}r_{+(LBH)}\left[(1-\Phi_E^2) + \frac{r_{+(LBH)}^2}{b^2} - 2\pi T r_{+(LBH)}\right]. \tag{C.8}$$

When large black hole solution dominates over the global AdS then $W < 0$. Using equation (C.6) which boils down to:

$$T > T_{o(M)} = \frac{1}{\pi b}\sqrt{1-\Phi_E^2}. \tag{C.9}$$

This bound is the maximum coexistence temperature (equation B.5), the temperature at which AdS and large black hole coexist at $B = 0$. Above $T_{o(M)}$, $\mathcal{M} = 0$ solution dominates, while below it $\mathcal{M} = \pm\sqrt{1-\Phi_E^2}$ dominates. But the latter two have the same free energy (equation C.8). Thus system has to spontaneously choose between these two solutions. As soon as B is applied one of the solutions disappears[5], and system has a preferred direction. This behaviour has similarity with ferromagnetic system.

Notice that the free energy is always zero in $B \to 0$ limit (except for $\mathcal{M} = 0$). However we can have some insight if we plot $W/|B|$ instead, which keeps the extremas of W unaltered[6] (figure 15).

Ideally one would be tempted to Taylor expand equation (C.3) near $\mathcal{M} = 0$, and construct a Landau-type model to see the symmetry breaking explicitly. However this is not feasible in our case, as $W/|B|$ is discontinuous and diverging at $\mathcal{M} = 0$ due to the inclusion of $|\mathcal{M}|$, and thus the Taylor expansion breaks down.

D. Details of diamagnetic and paramagnetic phases

Equation (5.8) gives behaviour of χ with B. Thus if we study χ at a constant magnetic field, system will be diamagnetic if:

$$3b^{10}B^2 + 3\mathcal{M}^4 - b^4\mathcal{M}^2\left(1-\Phi_E^2\right) < 0 \tag{D.1}$$

or

$$3b^{10}B^2 + \mathcal{M}^4 - b^4\mathcal{M}^2\left(1-\Phi_E^2\right) > 0 \tag{D.2}$$

and otherwise paramagnetic. That is diamagnetic solution is given by:

$$\mathcal{M} < \frac{b^4}{2}\left(\left(1-\Phi_E^2\right) - \sqrt{\left(1-\Phi_E^2\right)^2 - 12b^2B^2}\right) \tag{D.3}$$

[5]Since B and $\mathcal{M}$ must have opposite signs, one of the solutions of $\mathcal{M}$ vanishes depending on the sign of B.

[6]We cannot divide by B as its sign has a dependence on $\mathcal{M}$ due to positivity of r_+

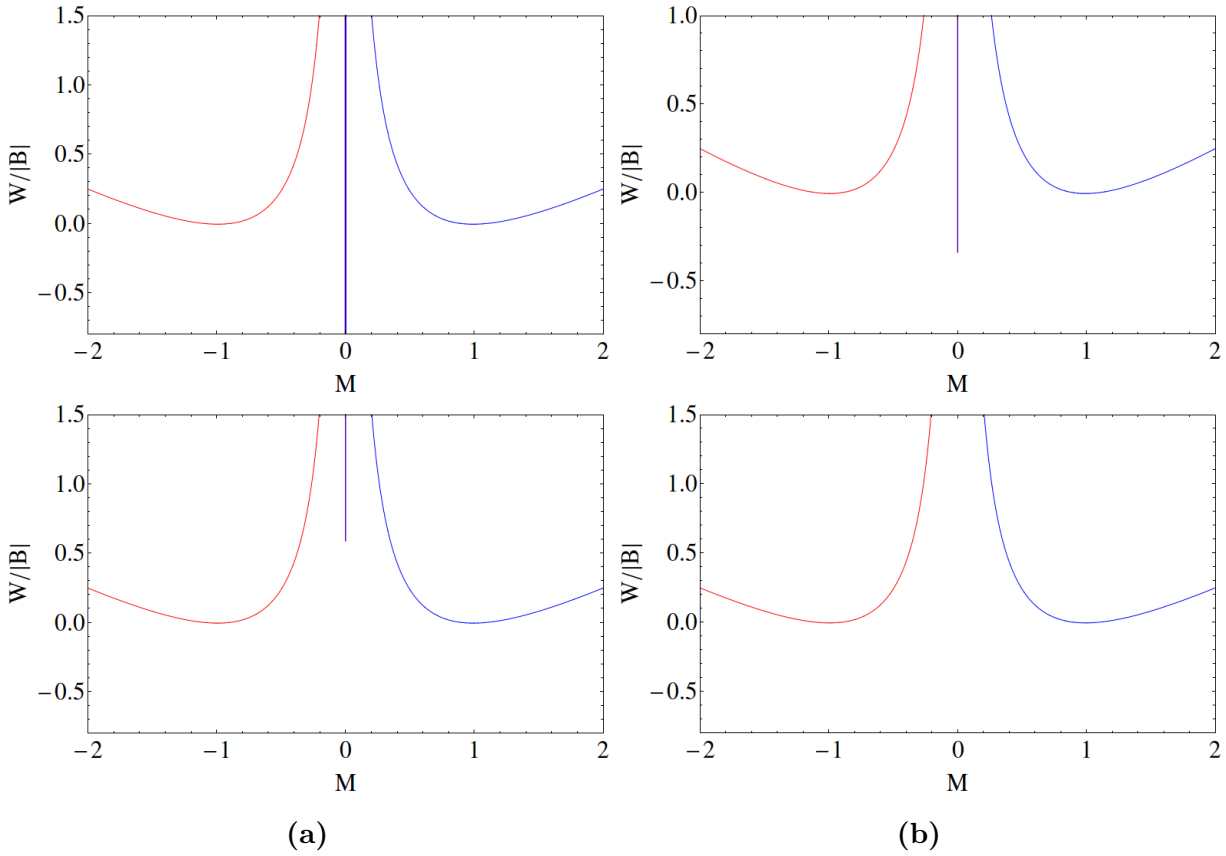

Figure 15: $W/|B|-\mathcal{M}$ graph for varying T ($\Phi_E = 0.1$) as $B \to 0$. Red curve is for $B \to 0^+$ while Blue is for $B \to 0^-$. In the first and second graph, $T > T_{o(M)}$ (coexistence temperature) and we see that the thermodynamics is governed by $\mathcal{M} = 0$ (Large BH) solution. As T is dropped below T_o (third graph), system spontaneously chooses between the two available solutions of $\mathcal{M} = \pm\sqrt{1-\Phi_E^2}$ (Small BH or background AdS) as both are equally likely. Further when T is decreased even below $T_{N(M)}$, the $\mathcal{M} = 0$ solution vanishes altogether (fourth graph).

$$\frac{b^4}{6}\left(\left(1-\Phi_E^2\right)-\sqrt{\left(1-\Phi_E^2\right)^2-36b^2B^2}\right) < \mathcal{M} < \frac{b^4}{6}\left(\left(1-\Phi_E^2\right)+\sqrt{\left(1-\Phi_E^2\right)^2-36b^2B^2}\right) \tag{D.4}$$

$$\mathcal{M} > \frac{b^4}{2}\left(\left(1-\Phi_E^2\right)+\sqrt{\left(1-\Phi_E^2\right)^2-12b^2B^2}\right). \tag{D.5}$$

The middle one is however the unstable phase. If,

$$|B| > B^* = \frac{1}{2\sqrt{3}b}\left(1-\Phi_E^2\right) \tag{D.6}$$

the system will always be diamagnetic regardless of temperature (figure 2a). However

if,

$$B^* > |B| > |B_c| \tag{D.7}$$

the system will have three phases: diamagnetic, paramagnetic and another diamagnetic (figure 2b).

If the magnetic field is even below B_c, system shows the full feature of 5 phases. But as we go below the critical point, we know that there comes an unstable branch which is omitted by the Maxwell's equal area law (figure 8). While we do so, a section of the small and large BH is also omitted. As a result below a particular magnetic field $B^{\#}$, the paramagnetic phase of large BH gets cutout and the only stable solution of large BH is diamagnetic phase. $B^{\#}$ will be given by the point where the coexistence magnetic field is same as the $\chi = 0$ point for a $B - \mathcal{M}$ isotherm. For $\Phi_E = 0$ and $b = 1$ we find $B^{\#} \approx 0.154$ whereas $B_c = 0.167$.

References

[1] J. M. Maldacena, Adv. Theor. Math. Phys. **2**, 231 (1998) [hep-th/9711200].

[2] E. Witten, Adv. Theor. Math. Phys. **2**, 253 (1998) [hep-th/9802150].

[3] S. A. Hartnoll, C. P. Herzog and G. T. Horowitz, Phys. Rev. Lett. **101**, 031601 (2008) [arXiv:0803.3295 [hep-th]].
S. A. Hartnoll, C. P. Herzog and G. T. Horowitz, JHEP **0812**, 015 (2008) [arXiv:0810.1563 [hep-th]].

[4] S. A. Hartnoll and P. Kovtun, Phys. Rev. D **76**, 066001 (2007) [arXiv:0704.1160 [hep-th]].

[5] M. M. Caldarelli, O. J. C. Dias and D. Klemm, JHEP **0903**, 025 (2009) [arXiv:0812.0801 [hep-th]].

[6] S. A. Hartnoll, P. K. Kovtun, M. Muller and S. Sachdev, Phys. Rev. B **76**, 144502 (2007) [arXiv:0706.3215 [cond-mat.str-el]].

[7] A. Chamblin, R. Emparan, C. V. Johnson and R. C. Myers, Phys. Rev. D **60**, 064018 (1999) [hep-th/9902170].

[8] D. Kubiznak and R. B. Mann, JHEP **1207**, 033 (2012) [arXiv:1205.0559 [hep-th]].

[9] N. Altamirano, D. Kubiznak, R. B. Mann and Z. Sherkatghanad, arXiv:1308.2672 [hep-th].

[10] D. Kastor, S. Ray and J. Traschen, Class. Quant. Grav. **26**, 195011 (2009) [arXiv:0904.2765 [hep-th]].

[11] S. Chen, X. Liu, C. Liu and J. Jing, Chin. Phys. Lett. **30**, , 060401 (2013) (6) [arXiv:1301.3234 [gr-qc]].

[12] H. Lu, Y. Pang and C. N. Pope, arXiv:1307.6243 [hep-th].

[13] M. Henneaux and C. Teitelboim, Phys. Lett. B **143**, 415 (1984).

[14] M.M. Caldarelli, G. Cognola and D. Klemm, [arXiv:hep-th/9908022].

[15] S. Wang, S-Q. Wu, F. Xie and L. Dan, Chin. Phys. Lett., 23 (2006) 1096, [arXiv:hep-th/0601147]

[16] Y. Sekiwa, Phys. Rev. D73 (2006) 084009, [arXiv:hep-th/0602269].

[17] E.A. Larran aga Rubio, [arXiv:0711.0012 [gr-qc]].

[18] B. P. Dolan, Class. Quant. Grav. **28**, 125020 (2011) [arXiv:1008.5023 [gr-qc]].

[19] B. P. Dolan, Phys. Rev. D **84**, 127503 (2011) [arXiv:1109.0198 [gr-qc]].

[20] V. Balasubramanian and P. Kraus, Commun. Math. Phys. **208**, 413 (1999) [hep-th/9902121].

[21] S. W. Hawking and D. N. Page, Commun. Math. Phys. **87**, 577 (1983).

[22] S. Surya, K. Schleich and D. M. Witt, Phys. Rev. Lett. 86, 5231 (2001) [arXiv:hep-th/0101134].

[23] N. Banerjee and S. Dutta, JHEP **0707**, 047 (2007) [arXiv:0705.2682 [hep-th]].

[24] E. Witten, Adv. Theor. Math. Phys. **2**, 505 (1998) [hep-th/9803131].

[25] M. Cvetic and S. S. Gubser, JHEP **9904**, 024 (1999) [hep-th/9902195].

[26] P. Basu and S. R. Wadia, Phys. Rev. D **73**, 045022 (2006) [hep-th/0506203].

[27] D. Yamada and L. G. Yaffe, JHEP **0609**, 027 (2006) [hep-th/0602074].